RESEARCH PAPER

Lateral Response and Failure Mechanisms of Rigid Piles in Soft Soils Under Geosynthetic-Reinforced Embankment

Anhui Wang[1] · Dingwen Zhang[1] 🔗

Abstract

Previous studies regarding geosynthetic-reinforced pile-supported (GRPS) embankments over soft soils have mainly focused on load transfer mechanisms and design approaches. However, little attention was given to the lateral performance of rigid piles in GRPS embankment systems. This paper presents the results of 3D finite element analyses to examine and compare the lateral response and failure mechanisms of floating and end-bearing piles in soft soils under geosynthetic reinforced embankments. The effects of geosynthetic reinforcement and pile length on the stability of the embankments are also investigated. The results indicate that the induced lateral responses in the piles are distinctly different for floating and end-bearing piles. Failure of the floating pile is primarily caused by the inclination of the pile. However, for end-bearing piles, bending failure is clearly established as the principal mode of failure. The benefit of the geosynthetic layers in improving the stability of piled embankments is not particularly apparent. Moreover, the increase in pile length is significant in enhancing the stability of GRPS embankments. Specifically, when the normalized pile length varies from 0.75 to 1.15, the critical height of embankment increases from 6.2 to 11.8 m. However, the effect of pile length becomes negligible when the normalized pile length exceeds 1.15. The lateral movement and failure modes of GRPS embankments are strongly dependent on pile length. Therefore, it is essential to consider this aspect when analyzing the stability of the GRPS embankment.

Keywords GRPS embankment · Floating pile · End-bearing pile · Lateral response · Failure mode

1 Introduction

Geotechnical engineers usually face several challenges when designing highway or railway embankments that are constructed on soft soils. These challenges, which mainly stem from the undesirable characteristics of soft soils, include intolerable settlement, potential bearing failure and global or local instability [1–3]. Thus, appropriate improvement techniques must be used for embankment construction over soft soils. Recently, a geosynthetic-reinforced pile-supported (GRPS) embankment system that efficiently combines vertical rigid piles (floating or end-bearing) and a horizontal geosynthetic-reinforced platform has emerged as a practical and reliable solution [4–6].

GRPS embankments have been successfully adopted globally in the construction of highways and railways, especially in cases where embankment deformation is a critical control item and where rapid construction of embankments is needed [6, 7].

A plethora of studies have been performed to investigate the fundamental performance of GRPS embankments based on small-scale models [4, 6, 8], full-scale field tests [9–11], numerical modeling [12–15], and theoretical models [16–19]. According to previous studies, it is evident that the load transfer mechanism in such systems is comprised of a combination of soil arching phenomena, as well as the tensioned membrane effects of the geosynthetic reinforcement, wherein a majority of the embankment load is transferred from the soft soils to the piles. Fortunately, a variety of approaches have also been successfully developed for predicting the bearing resistance of the pile [20–23]. Notably, when constructing GRPS embankments over soft soils, pile caps are usually employed to facilitate the transfer of more embankment loads to the piles, therefore, allowing for larger pile spacing [6, 16]. In such cases,

✉ Dingwen Zhang
zhangdw@seu.edu.cn

Anhui Wang
230169700@seu.edu.cn

1 School of Transportation, Southeast University,
Nanjing 211189, China

rigid piles are also required to provide sufficient passive resistance to limit lateral movement of the soils. Therefore, further research is necessary to assess the lateral response of rigid piles in soft soils under geosynthetic-reinforced embankments.

Currently, several model tests and numerical simulations have been performed to examine the pile lateral behavior of rigid pile-supported embankments [24–26]. Based on these studies, the possible failure modes of rigid piles under embankment loads have been identified mainly as bending and inclination failures. However, the conditions that prompt bending or inclination failure of rigid piles in the GRPS embankment system are not yet clear. Additionally, the influence of pile length on the lateral movements of rigid piles under geosynthetic-reinforced embankment has been seldom reported. As a result, systematic studies of the lateral behavior and failure modes of rigid piles in supporting geosynthetic-reinforced embankment over soft soils are required.

Based on a case history of a GRPS highway embankment project, a three-dimensional (3D) numerical modeling of the GRPS embankment was established using the ABAQUS finite element (FE) software, which took into account pile–soil and geosynthetic-gravel interactions. The numerical results that were initially validated against the field measurements were utilized to discuss and evaluate the lateral behaviors and failure modes of floating and end-bearing piles under geosynthetic-reinforced embankments. Furthermore, the effects of geosynthetic reinforcement and pile length on the stability of embankments were examined.

2 Site Conditions and Project Overview

A highway embankment project was implemented at a site located in a northern suburb of Wuhan, China. The project site lies in the Jianghan plain-lake district of the middle and lower Yangtze River, and is mainly covered by Quaternary alluvium deposits. Extensive field tests and laboratory tests were conducted there to characterize the subsoil conditions. Specifically, conventional laboratory soil tests were carried out to determine the unit weight, water content, void ratio, compression modulus and relevant shear parameters of the foundation soils. Additionally, a vane shear test, which is one of the most widely used field tests in geotechnical investigations, was performed to evaluate the undrained shear strength of the soft soil layer. Figure 1 summarizes the available detailed test data of the soil properties. Evidently, the project site consists of silty clay lying virtually from the ground surface to a depth of about 20 m, which is underlain by a layer of silty sand. The upper layer signifies the main soft soil layer and is characterized by high compressibility and low strength. The initial bearing resistance of the soft soil ground approaches 100 kPa. Below the soft soil layer, there is a stiff soil layer, exhibiting a substantially higher strength and an initial bearing resistance of 300 kPa. The water level is approximately located at the ground surface. Additionally, it is worth mentioning that the undrained shear strength of the soft soil layer displayed a minimum value at ground surface level and gradually increases with depth.

Given the poor subsoil conditions at the project site and the limited construction period, a GRPS embankment system was adopted for this project to improve the bearing capacity of the soft ground and reduce the embankment settlement. According to the design scheme, the
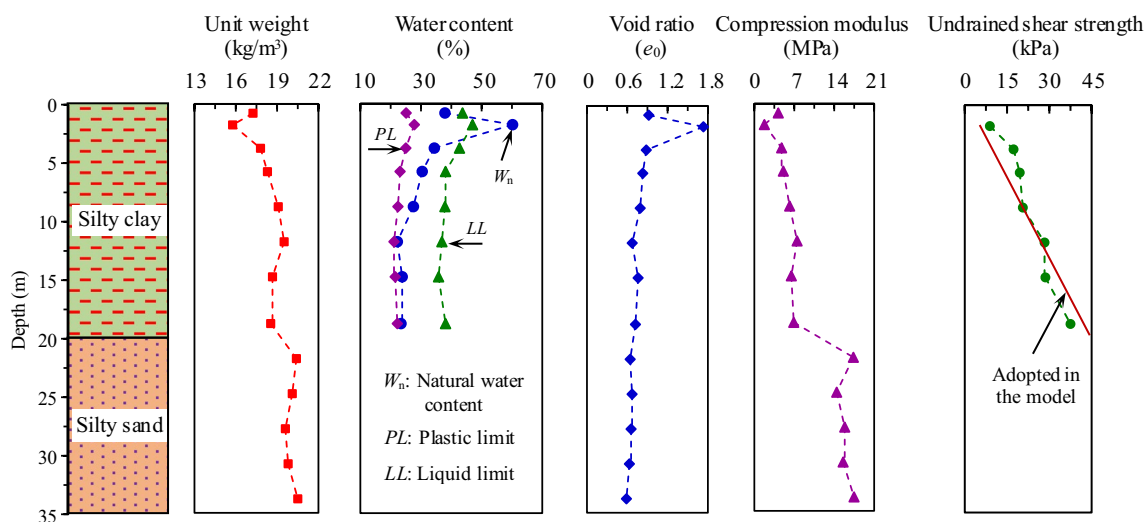

Fig. 1 Soil profile and engineering properties of the test site

embankment was 7.5 m high with a crest width of 26 m, while the side slope was 1 V: 1.5 H. The fill material consisted mainly of sandy soil with a friction angle of 35° and an average unit weight of 20 kN/m³. The embankment was supported by pretensioned high-strength concrete (PHC) piles with exterior diameters of 0.4 m, which were arranged in a square pattern with a center-to-center spacing of 2.5 m. Considering the economy, these rigid piles were designed to be 15 m in length, and the pile tips did not reach the stiff soil layer; that is, floating piles were used in the GRPS embankment. Once installation of the PHC piles was completed, the square pile caps with dimensions of 1 m × 1 m × 0.3 m (length × width × thickness) were cast in the field. According to the work of Liu et al. [5] and Zhang et al. [7], a geosynthetic-reinforced gravel layer with a thickness of 50 cm was laid over the pile caps to provide a working layer and increase the soil arching effect, where double geosynthetic layers were placed as an interlock with the gravel fill. The tensile stiffness and strength in both longitudinal and transverse directions of the geosynthetics were 1500 kN/m and 120 kN/m, respectively. Figure 2a illustrates the typical cross section of the GRPS embankment and arrangement of piles. Additionally, to monitor the settlement response of the GRPS embankment during construction, surface settlement plates were installed at the center line of the embankment.

The embankment construction stage was planned to last for only 30 days, and the average filling rate was about 0.25 m/day. However, when the embankment was filled to a height of approximately 6.2 m, the settlement and lateral movement of the GRPS embankment exhibited a substantial increase, inducing a sudden collapse failure to occur (as shown in Fig. 3a). Essentially, the embankment failure height was approximately 6.2 m, just below the design height of 7.5 m. According to field observations, the floating PHC piles close to the embankment toe did not exhibit obvious signs of settlement, but there were 0.6–0.8 m lateral movements at the heads of these piles. More importantly, the failure of these floating piles was clearly identified as an inclination failure. As a result, the cause of the GRPS embankment failure was mainly attributed to the insufficient lateral resistance provided by the floating piles in the soft soils, as schematically drawn in Fig. 2a. The failure mechanism mentioned above was demonstrated by the numerical results presented in this paper. However, based on the existing design approaches provided by the relevant specifications [27, 28], these floating piles were sufficient to control both the total settlement and instability of the GRPS embankment. This suggests that the existing design approaches resulted in a non-conservative prediction of GRPS embankment stability and should, therefore, be treated with the appropriate caution. Detailed discussions in this regard will be provided in later sections.

To deal with the GRPS embankment's collapse failure, a remedial measurement (i.e., increasing the pile length) was proposed for implementation during the reconstruction of the geosynthetic-reinforced embankment. Specifically, end-bearing piles with lengths of 23 m were installed to support the geosynthetic-reinforced embankment, as shown in Fig. 2b. In this case, the embedded length of end-bearing piles in the stiff soil layer was 3.0 m. Compared with the floating piles, applying the end-bearing piles was expected to increase the passive resistance, thereby limiting lateral movement of the GRPS embankment. As expected, using the end-bearing piles, the highway embankment (with a height of 7.5 m) was safely reconstructed over the soft soils without causing any global or local instability (as seen in Fig. 3b). Consequently, it may be inferred that the use of end-bearing piles clearly reduced the lateral displacements and enhanced the stability of the GRPS embankment.

3 Numerical Modeling and Validation

3.1 FE Modeling

The analysis of a GRPS embankment is truly a three-dimensional (3D) problem. In this study, numerical analyses were performed using the general FE platform ABAQUS under 3D conditions. However, considering symmetry, it is possible to select only one half of the GRPS embankment and only a 3D slice unit for numerical modeling. The 3D model and FE mesh that were adopted are illustrated in Fig. 4. The modeled volume was 70 m by 2.5 m in the horizontal plane and 35 m in depth from the ground surface. In this case, the boundary effect can be minimized. It is worth noting that a 2.5 m wide section with one row of piles was selected in the longitudinal direction of the embankment for simplicity. The bottom of the model was fixed against displacement in all directions, and the other four vertical sides were allowed to move freely in-plane; however, out-of-plane movement was prohibited. Additionally, only the ground surface and the bottom boundaries (silty sand layer) were considered completely permeable, while the other four boundaries were considered to be impermeable. Considering the coupled effect of the embankment filling and soil consolidation, eight-node trilinear displacement and pore pressure elements were adopted in the 3D model to represent the foundation soil. The gravel layer, embankment fill and piles were all modeled using eight-node linear brick elements. Moreover, the geosynthetic layer was modeled using eight-node quadratic, reduced integration membrane elements with a capacity to resist only tensile force. In particular, the total number of elements was approximately 254,000 in simulating the GRPS embankment. Regarding the convergence to the exact solution, an additional numerical analysis demonstrated that
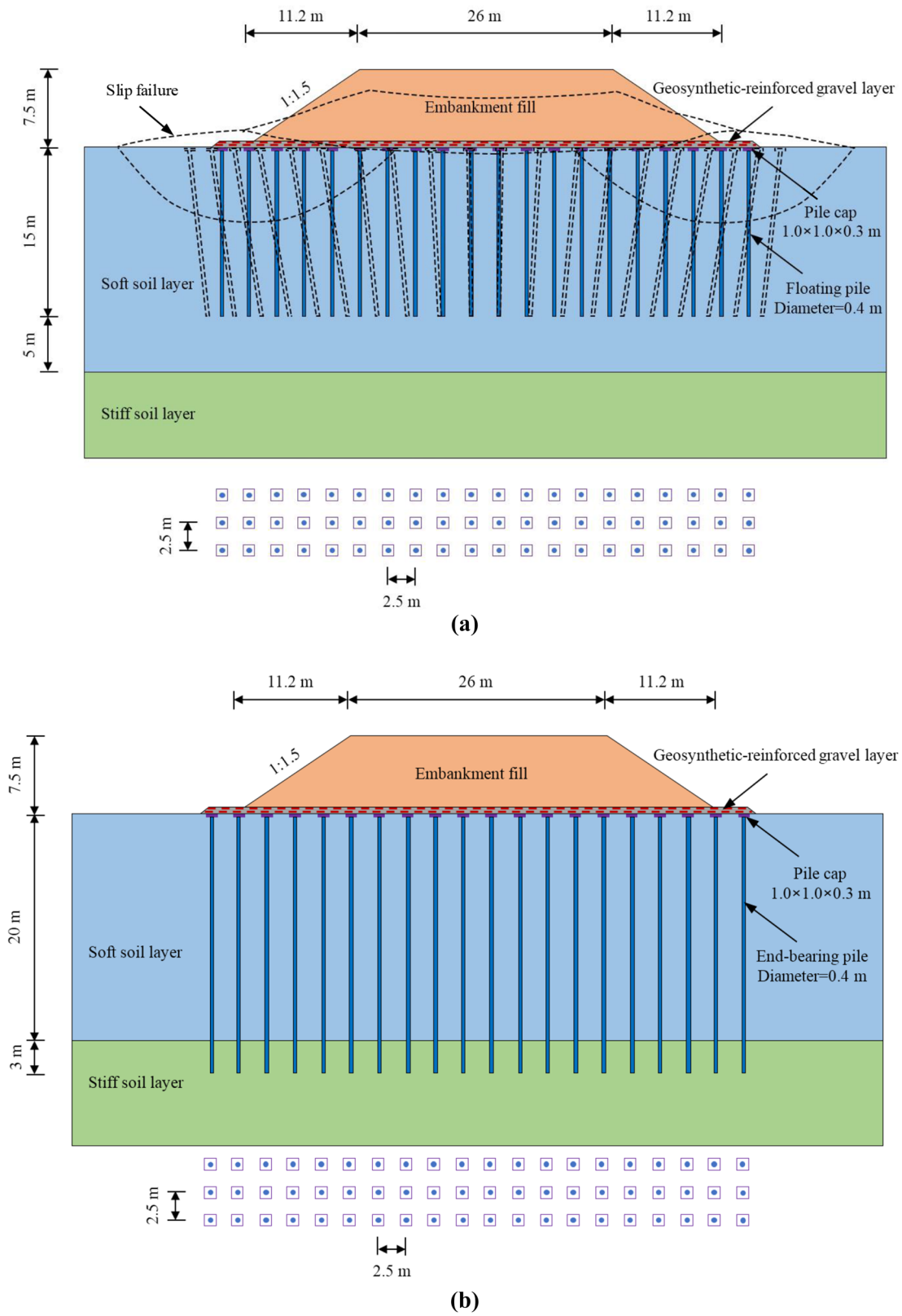
Fig. 2 Cross section of GRPS embankment and layout of rigid piles: **a** floating pile case and **b** end-bearing pile case

(a)   **(b)**

Fig. 3 **a** Failed highway embankment supported on floating piles; **b** completed highway embankment supported on end-bearing piles

further halving the current mesh size may only result in a negligible change of less than 1.0% in the computed results. This suggests that the fineness of the mesh used for the 3D model was sufficient.

The FE analyses consisted of two primary steps. First, all the elements corresponding to the embankment fill were removed, and the initial stress field of the pile–soil domain was balanced by applying a body force equal to the weight of the pile–soil system. Then, these elements were added in successive layers of 0.25 m in height (0.25 m/day) to simulate the embankment construction process until the total height of the embankment was reached. Moreover, to account for the large deformation effect on the GRPS embankment, all analyses were conducted using an arbitrary Lagrangian–Eulerian (ALE) technique in which the high-quality meshes would be maintained during the embankment loading. A detailed description of the ALE approach is provided in the ABAQUS technical manual.

3.2 Material Models and Parameters

It is well-known that the modified Cam Clay (MCC) model is able to capture the essential deformation and failure characteristics of soft soils under drained conditions [29–31]. Therefore, the MCC model was adopted in this study to simulate the elasto-plastic behavior of the silty clay. In MCC model, four main material parameters are required, which include the slope of the virgin consolidation line (λ), the slope of the swelling line (k), the void ratio at unit pressure (e_1), and the slope of the critical state line (M). Specifically, values for λ and k were determined from the results of one-dimensional consolidation tests with a vertical stress of 100–200 kPa. The values of e_1

were deduced according to the MCC model and the results of the one-dimensional consolidation tests. The value of M was obtained from the results of the consolidated und-rained triaxial tests. The silty sand layer, embankment fill and gravel layer were modeled as perfectly elasto-plastic materials following a Mohr–Coulomb (MC) failure criterion. Based on the work of many scholars (e.g., Han and Gabr [1], Liu et al. [5], Zhang et al. [32], Rowe and Liu [33], Bhasi and Rajagopal [34]), the rigid piles and geosynthetic layer were assumed to be linear elastic (LE) materials. It should be noted that the elastic modulus of the geosynthetic can be expressed as the tensile stiffness divided by the thickness. Moreover, the thickness of the geosynthetic reinforcement was assumed to be 2.0 mm in the model, which is the typical thickness used in the practice. Therefore, the elastic modulus of the geosynthetic equaled 750 MPa. The material models and the related model parameters used in this study are listed in Table 1. It is worth mentioning that for each soil layer, the theoretical values of undrained shear strength by the MCC model increase linearly with depth, as reported by Liu et al. [5] and Wu et al. [31]. According to the soil parameters used, the undrained shear strength of the silty clay adopted in the numerical modeling is presented as the solid line in Fig. 1.

The interface behaviors of pile–soil and geosynthetic-gravel are vital for the performance of the GRPS embankment system. Hence, their contact behaviors were defined using an isotropic Coulomb friction model, which allows for slippage and separation between the master and slave surfaces. In the analyses, the typical friction coefficients of 0.3 and 0.7 were applied for the pile–soil and geosynthetic-gravel interfaces, respectively, based on the friction angles of soft soils and gravel.
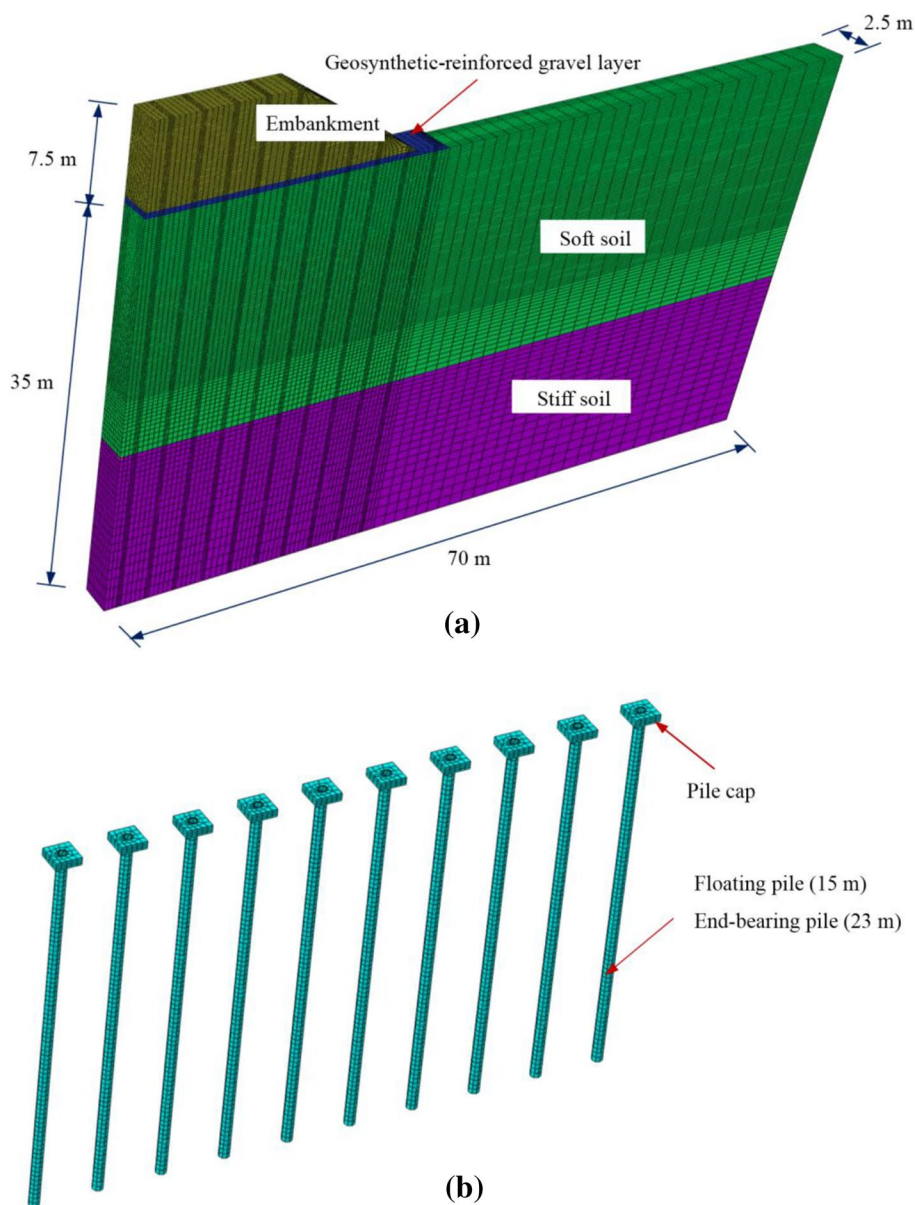
Fig. 4 3D finite element mesh of **a** full model and **b** pile model

Table 1 Material models and related model parameters adopted in this study

Material type	Model	γ (kN/m^3)	E (MPa)	ν	c (kPa)	Φ (°)	λ	k	M	e_1	k (10^{-4} m/day)
Silty clay	MCC	18.0	–	0.40	–	–	0.084	0.017	1.1	1.05	4.5
Silty sand	MC	20.0	20	0.35	10	30	–	–	–	–	150
Embankment fill	MC	20.0	25	0.30	8	35	–	–	–	–	–
Gravel layer	MC	20.0	35	0.30	2	40	–	–	–	–	–
Rigid pile	LE	25.0	3.8×10^4	0.15	–	–	–	–	–	–	–
Geosynthetic	LE	–	750	0.30	–	–	–	–	–	–	–

γ unit weight, E Young's modulus, ν Poisson's ratio, c cohesion, Φ friction angle, k permeability coefficient

3.3 Validation of the Model

To verify the feasibility of the numerical model used in the present study, Fig. 5 compares the field measurements and numerical predictions of the settlement response at the base of the GRPS embankment. Since the filling height of the GRPS embankment was 7.5 m, only the measurement results for the embankment height ranging from 0 to 7.5 m are presented in Fig. 5. It can be seen from the figure that the predicted settlements were slightly smaller than that measured under different embankment heights; however, there was an acceptable agreement between them. In particular, the numerical model adopted in this study captured the nonlinear steep change in the two such curves for the cases of embankments supported on floating and end-bearing piles, demonstrating that the material properties and constitutive models are capable of appropriately modeling the deformation behavior and failure process of the GRPS embankment system.

To examine whether the weak interaction of gravel soil and geosynthetic reinforcement would result in the embankment failure, an additional numerical model was established for simulating the fully bonded behavior between these two elements. Specifically, the interface between gravel and the geosynthetic layer was modeled using embedded contacts without considering the slip failure between them. The results from Fig. 5 show that the predicted settlement response using the embedded contacts was essentially no different from that of the Coulomb friction model, implying
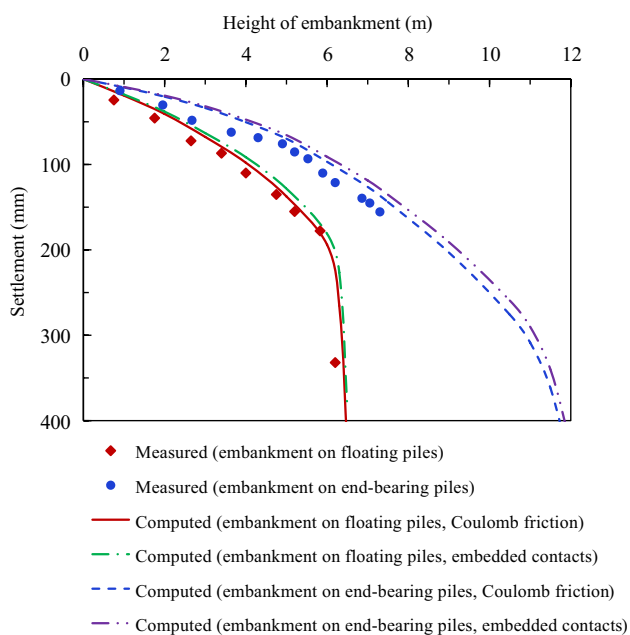
that the embankment failure was not caused by the weak interaction of gravel soil and geosynthetic layers. Actually, according to the filed and numerical investigations, the failure of the GRPS embankment was due to the insufficient pile length, which did not provide sufficient lateral resistance to prevent the substantial lateral movement of the soft soils. In other words, the insufficient pile length induced the failure of the floating piles and the soft foundation soils under embankment loads, a topic to be discussed in the following sections.

4 Numerical Results and Analyses

Generally, the lateral movement and bending moment of piles under embankment loading increased from the central piles (close to the center of the embankment) to the side piles (under embankment slope and close to the embankment toe), which has previously been verified by Su and Huang [24]. In other words, the side piles were more severely affected by the lateral displacement of soft soils, increasing the likelihood of the GRPS embankment collapsing due to the failure of the side piles. Therefore, for simplicity, the lateral responses of the floating and end-bearing piles under the toe of the GRPS embankment were compared and analyzed.

4.1 Lateral Movements Along Pile

Figure 6a, b shows the computed lateral movement profiles along the depths of the floating and end-bearing piles, respectively. It is seen that the lateral movement along the floating pile approximately decreased linearly from the pile head, whereas the lateral movement along the end-bearing pile apparently decreased nonlinearly from the pile head. Evidently, larger movement amplitudes for these two cases occurred in the upper portion of the piles. In addition, the lateral movements increased gradually with increasing embankment heights, irrespective of pile type. However, the lateral movements of the end-bearing pile were visibly less than that of the floating pile at various heights of the GRPS embankment.

The maximum lateral movements of these two types of piles were compared at various embankment heights, and the maximum lateral movement versus the embankment height plots are presented in Fig. 7. It is clear that after reaching a certain embankment height, both the floating and end-bearing piles displayed a sharp increase in maximum lateral movement, which indicated the significant risk of instability regarding the GRPS embankment. In terms of the instability of GRPS embankments, the lateral failure of the pile–soil system can result from the lateral failure of the rigid piles followed by the yielding of the soft surrounding soils. As discussed, the MCC model used in this study is capable of
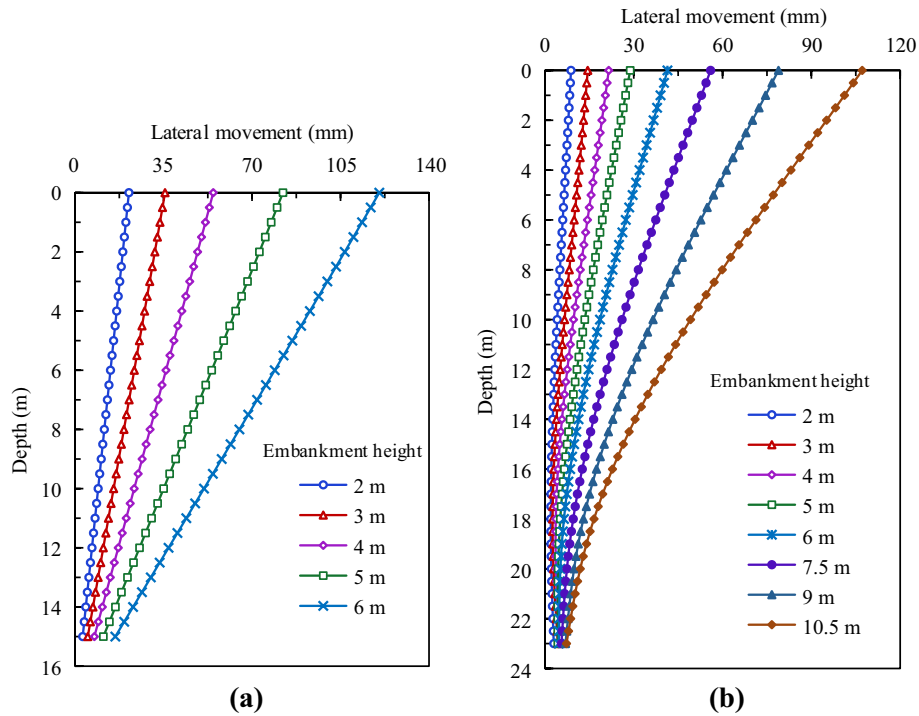

Fig. 5 Measured versus computed settlements at the embankment base

Fig. 6 Computed lateral movement profiles along the depths of the **a** floating and **b** end-bearing piles
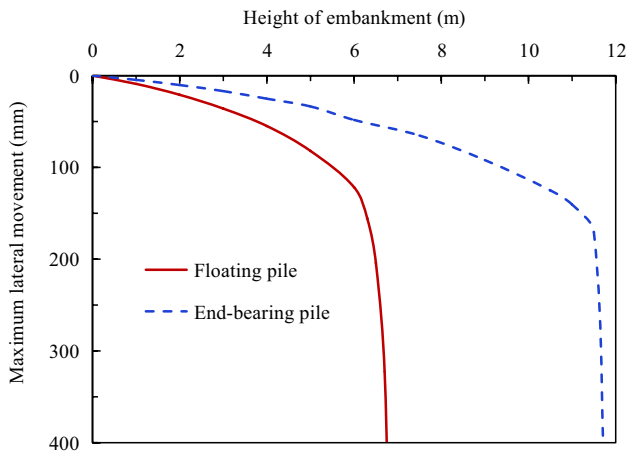

Fig. 7 Maximum lateral movement versus embankment height response

representing the steep change in lateral movement versus embankment height curves (as shown in Fig. 7), indicating that the lateral failure of soft soils due to the embankment loads was successfully predicted. For the floating pile, once the embankment height exceeded 6.0 m (i.e., the maximum lateral movement of the floating pile reached 122 mm), the failure of the pile and soft surrounding soils occurred and resulted in the collapse failure of the GRPS embankment. However, in the case of the end-bearing pile, the failure height of the GRPS embankment increased to about 11.5 m.

It is also worth mentioning that the maximum lateral movement of the end-bearing pile was only 48 mm at an embankment height of 6.0 m, which is 61% lower than that of the floating pile. Similar behavior was also detected at a lower embankment height.

It is evident from Fig. 6a that for the floating pile of 15 m, though the lateral movement of the pile head was markedly larger than the end, about 16 mm of outward lateral movement at the end of the pile at an embankment height of 6.0 m still existed. However, the end-bearing pile was installed to a depth of 23 m from the ground surface, and it was found that there was negligible lateral movement at that particular depth. This can be attributed to the fact that the end-bearing pile was sufficiently embedded in a stratum, which exhibits much stiffer lateral response, and consequently, the effect of embedment may have played a key role in reducing the lateral movement of the pile. Thus, it can be concluded that, compared with floating piles, applying end-bearing piles reduces the lateral movement of piles to a considerable extent. This also clearly aligns with the notion that the stability of the GRPS embankment may be clearly improved using end-bearing piles instead of floating piles. In this sense, the reinforcement effect of the end-bearing piles is significantly preferred over that of floating piles. Of course, it should also be noted that an end-bearing pile could have sufficient axial resistance with little or no embedment into a stiff soil layer but still have insufficient lateral resistance if it is not sufficiently embedded into that layer.

4.2 Bending Moments Along Pile

The computed bending moments in the floating and end-bearing piles under the toe of the GRPS embankment are presented in Fig. 8a, b, respectively. To distinguish the directions of the bending moments, the results were recorded as positive and negative. As indicated, the positive moment was revealed in the upper portion of the two types of piles. This result is ascribed to the composition of the pile cap and the geosynthetic-reinforced gravel layer that possesses a high rigidity and restrains the pile head to a certain extent. However, a distinct difference remained relating to the moment distribution between them. For the floating pile, the positive moment developed along the pile shaft which was located at a depth of about 13.5 m from the top of the pile. Therefore, the positive moment extended for almost the entire length of the pile. However, in the case of the end-bearing pile, the neutral plane, which refers to the change from a positive moment to a negative moment, was located at a depth of about 3.5 m. This difference may be attributed to the critical role of the pile type in the lateral response of the rigid pile under embankment loading. Moreover, the positive moments of the floating pile were higher than that of the end-bearing pile that was subjected to equal embankment loading. Furthermore, it should be noted that when the rigid pile was floated, the absolute maximum moment in the lower part of the pile was much smaller than in the upper part.

For the end-bearing pile, the absolute maximum moment occurred in the lower part of the pile, specifically at or near the interface between the alternating soft and stiff soil layers. Additionally, the bending moments of the end-bearing pile were approximately equal to zero at or near the end of the pile.

Under various embankment heights of 2, 3, 4, 5 and 6 m, the absolute maximum moments in the floating pile were about 15, 23, 32, 44 and 58 kN m, respectively, while for the end-bearing pile case, the absolute maximum moments were about 21, 35, 49, 65 and 83 kN m, respectively. It is apparent that the bending moments of the end-bearing pile were greater than those of floating pile under the same embankment loading, especially when the embankment load and lateral movement of the pile was large. It is considered that the stronger embedment effect of the end-bearing pile is an important reason for the larger bending moment predicted in Fig. 8b. In other words, the end-bearing pile serves as a reinforcing measure to prevent the soft soil surrounding it from experiencing significant lateral displacement. By doing so, lateral movements of the pile and soft soils should have been minimized, leading to an increased stability of the GRPS embankment. It is worth noting that when applying the end-bearing piles under the toe of embankment, one must design the piles with sufficient bending resistance to perform their intended function of enhancing the lateral stability of the embankment without being subject to bending failure.
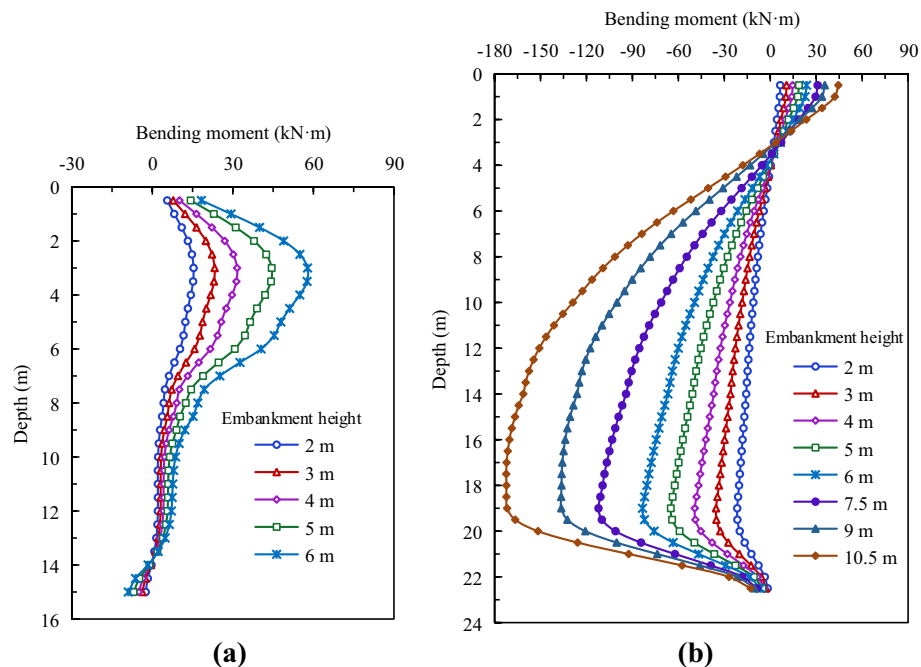

Fig. 8 Computed section moments along the depths of the **a** floating and **b** end-bearing piles

4.3 Failure Modes of Rigid Piles

To determine whether the shear failure would occur in the floating and end-bearing piles, the predicted shear forces in the two types of piles under various embankment heights are presented in Fig. 9a, b, respectively. The numerical results indicate that the two piles displayed different tendencies during the embankment loading. The maximum shear force in the floating pile was distributed through the upper portion of the pile, while this distribution occurred in the lower part of the end-bearing pile. Furthermore, compared with the floating pile, the end-bearing pile achieved a 50% increase in maximum shear force at an embankment height of 3 m and a 40% increase at an embankment height of 6 m. This result also indicated a noticeable difference in the lateral behavior of the floating and end-bearing piles. Nevertheless, it should also be noted that at various loading levels, the induced peak shear forces in these two piles were considerably lower than the shear strength of the piles (i.e., 276 kN). This result implies that for the high-strength rigid piles in soft soils under embankment loading, shear failure would generally not occur if either floating or end-bearing piles were used. Of course, it is essential to design both piles with adequate shear capacity to resist the anticipated shear loading. Moreover, the shear demand in end-bearing piles is typically larger than that in floating piles. It is also worth noting that the buckling instability is one of the most destructive elements for slender piles. For the floating and end-bearing piles in

the engineering case, the critical buckling loads can be at least 1708 kN and 960 kN, respectively, which were calculated using the Euler buckling formula without considering the effect of the lateral soil resistance. However, under the GRPS embankment loads, the induced maximum axial loads acted on the floating and end-bearing piles were about 98 kN and 191 kN, respectively, which were significantly smaller than their critical buckling loads. Therefore, the buckling of the two types of piles would not emerge during the embankment loading.

The simulated lateral movements of geosynthetic-reinforced embankments supported on floating and end-bearing piles are shown in Fig. 10a, b, respectively, from which it is seen that there was a noticeable difference in the deformation mode predicted for the two types of rigid piles. Moreover, the failure behavior of the pile is most likely to be influenced by the deformation mode, which also implies larger differences in the failure modes of floating and end-bearing piles. As illustrated in Fig. 8a, no large bending moments were observed in the floating pile, despite the large lateral movement along the pile. Specifically, the induced peak moment in the floating pile was significantly lower than the ultimate flexural strength of the pile (i.e., 159 kN m), even when the GRPS embankment was filled to its failure height. It can be seen in Figs. 8a and 10a that, under various embankment loadings, the floating pile remained virtually straight along its length, and significant inclination deformation occurred at large embankment heights. Thus, it may be inferred that
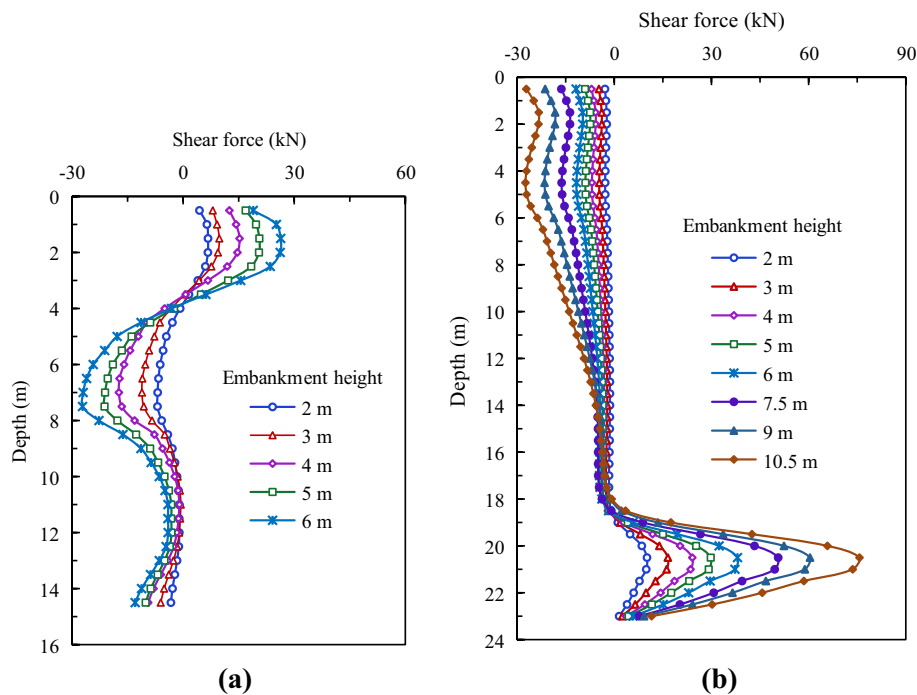

Fig. 9 Computed shear force distribution along the depths of the **a** floating and **b** end-bearing piles
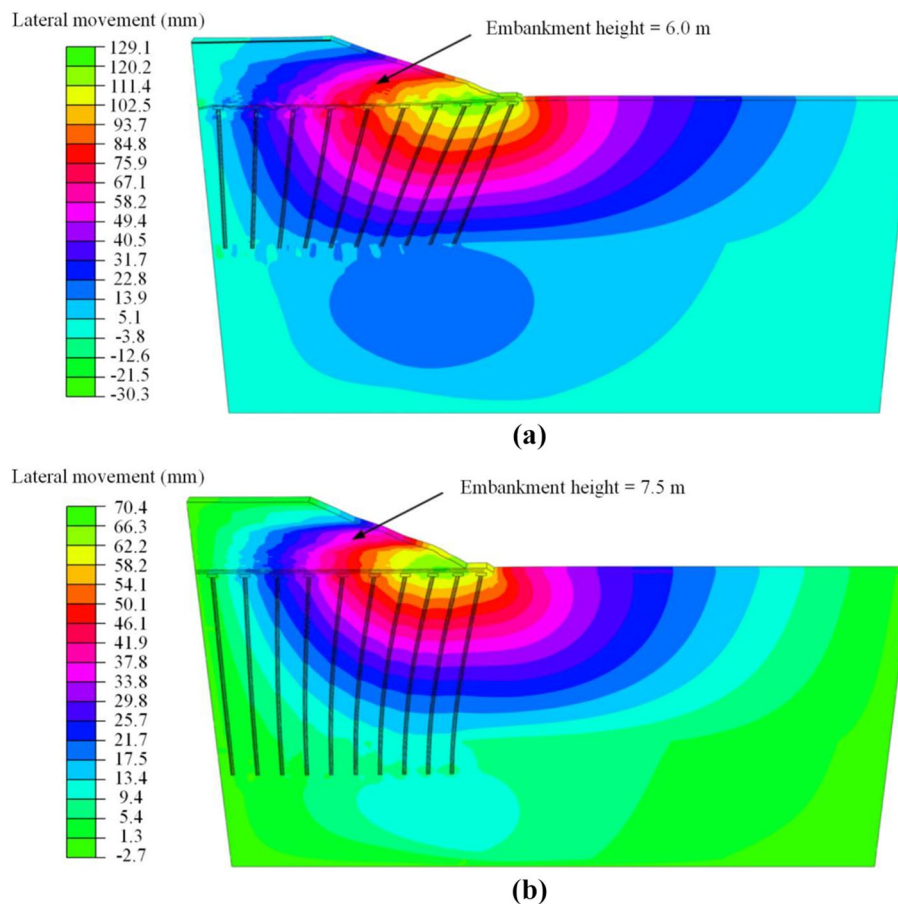
Fig. 10 Lateral movement contours of the GRPS embankments: **a** floating pile case and **b** end-bearing pile case

failure of the embankment is primarily caused by the inclination of the floating pile rather than the structural failure of the pile. However, with an increase in embankment height, the induced moments in the end-bearing pile remarkably increased, especially when the height of the embankment exceeded 7.5 m, as shown in Fig. 8b. Specifically, a maximum moment of 172 kN m was generated in the end-bearing pile at an embankment height of 10.5 m, which exceeded the flexural strength of the pile and would undoubtedly result in bending failure of the pile. It should be noted that the location of the bending failure initially occurred at or near the interface of stiff–soft soil layers. In such cases, the flexural strength of the pile at that location would have been sufficiently exerted to resist the lateral soil movements induced by embankment loads. Additionally, the simulated results from Figs. 8b and 10b clearly demonstrate the bending deformation of the end-bearing pile.

From these observations, it can be concluded that for the floating pile installed in soft soils and acted upon by geosynthetic-reinforced embankment loads, inclination failure occurs easily due to the substantial lateral movement of soft soils. The failure pattern also aligns with the studies of Kitazume and Maruyama [35] and Shrestha et al. [36], who found that, under embankment loading, all floating columns with a relatively high modulus inclined like dominos, and no bending failure occurred in the columns. Instead, the end-bearing pile does not fail by inclination but fails by a pattern of bending failure. At present, it is a common and popular practice to use the end-bearing piles to support the geosynthetic-reinforced embankment over soft soils. However, floating piles in very thick soft soils are more economical and technically feasible than the end-bearing piles [34]. As presented by Bhasi and Rajagopal [34], at large depths of soft soils, the use of floating piles can significantly decrease the lateral movement and settlement of the GRPS embankment. Of course, It should also be noted that compared with the end-bearing pile, the flexural strength of the floating pile cannot be sufficiently utilized under the embankment loading, which makes it uneconomical for application in soft soils considering the stability of the GRPS embankment. Moreover, when predicting the stability of piled embankments constructed on floating and end-bearing piles, various theoretical approaches should be considered due to a

profound difference in lateral failure mode between the two types of piles.

5 Discussions

5.1 Effect of Geosynthetic Reinforcement

It is widely recognized that in a GRPS embankment system, the inclusion of the geosynthetic reinforcement can transfer a higher vertical load from the soft soils to the rigid piles and consequently reduce the settlement and lateral movement of the soft soils. The tension change in the geosynthetic as a function of the distance from the center of the embankment is shown in Fig. 11 for both cases of floating and end-bearing piles. It is evident that the distribution of tension along the geosynthetic was not uniform and the larger tension always occurred at the edge of each pile. This finding is consistent with the observations made by Han and Gabr [1], and Liu et al. [5]. A comparison of Fig. 11a, b indicates that when the embankment height was less than 4.0 m, the tension in the geosynthetic for the case of end-bearing piles

was slightly larger than that for the case of floating piles. However, when the embankment height exceeded 4.0 m, the higher tension occurred in the geosynthetic for the case of floating piles. On the one hand, increasing the pile length promotes the development of differential settlement between the pile and surrounding soft soils, resulting in elevation of the tension; On the other hand, the larger lateral movement of the soft soils outward from the center of the embankment contributes to a higher tension. As a result, the change in the tension of the geosynthetic relies on the combined effect of differential settlement and lateral movement of the soft soils, which aligns with the findings from the field measurements and numerical investigations by Huang et al. [12]. Additionally, it should be noted that under higher loading levels, the maximum tensions generated in the geosynthetic for both cases were close to the tensile strength of the geosynthetic (i.e., 120 kN/m). Evidently, the efficacy of the geosynthetic reinforcement in resisting settlement and lateral movement of the soft soils has been well mobilized, especially under larger lateral movement.

Figures 12 and 13 demonstrate the influence of the tensile stiffness and number of geosynthetic layers on the maximum lateral movement of floating and end-bearing piles, respectively. It is seen that the higher tensile stiffness of the geosynthetic layers yielded a relatively smaller maximum lateral movement, irrespective of pile type. Similarly, an increase in number of the geosynthetic layers slightly reduced the maximum lateral movement of these two types of piles. The results can be explained by the increase in pile–soil stress ratio, leading to a decline in the lateral soil stress acting on the passive pile. Moreover, it was observed that the effect of the tensile stiffness and number of geosynthetic layers on the lateral movement in both cases became negligible when the tensile stiffness exceeded 3000 kN/m and the number of
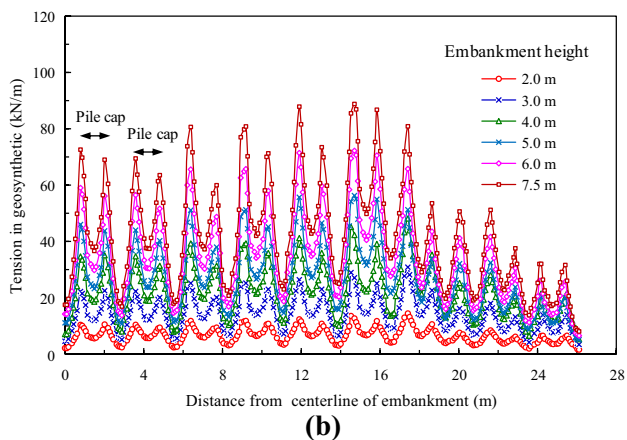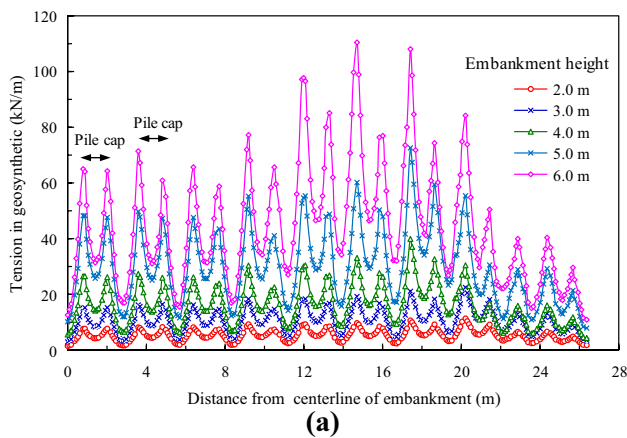

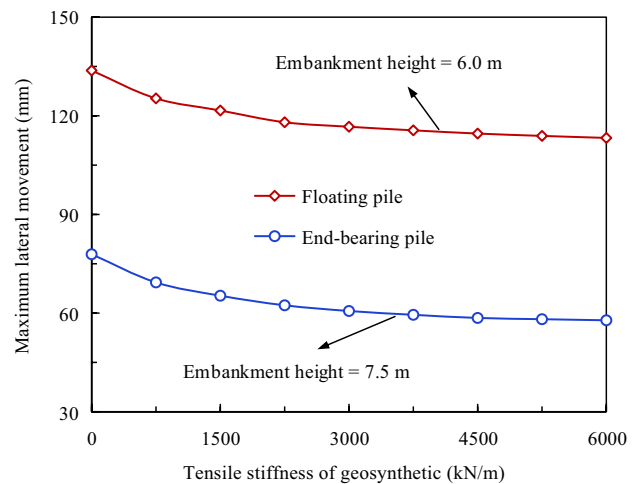**Fig. 11** Distribution of tension in geosynthetic for both cases of **a** floating and **b** end-bearing piles

Fig. 12 Influence of geosynthetic stiffness on maximum lateral movement of the floating and end-bearing piles
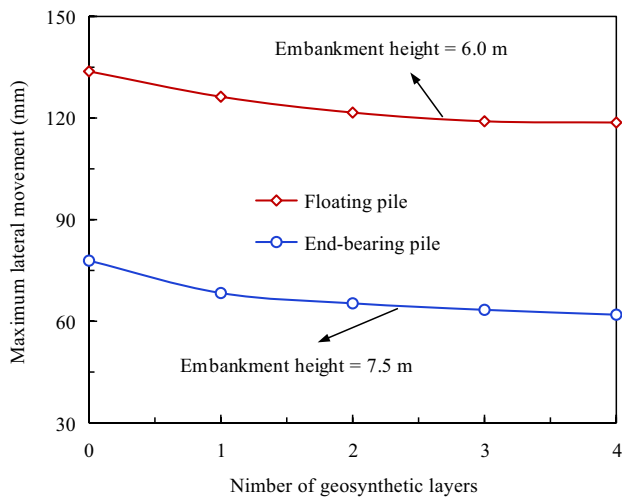
Fig. 13 Influence of number of geosynthetic layers on maximum lateral movement of the floating and end-bearing piles

the geosynthetic layers was more than 2. It should also be noted that the benefit of the geosynthetic layers in reducing the lateral movement of rigid piles is limited. In other words, the effect of geosynthetic layers on the stability of GRPS embankments is not very significant.

5.2 Effect of Pile Length

Typically, the spacing and location of the rigid piles have a noticeable effect on the displacement of the GRPS embankment. However, according to the optimum design for GRPS embankments by many scholars [15, 16, 19, 37], the pile spacing is proposed to be 3–5 times the pile diameter (without pile cap) and 6–8 times the pile diameter (with pile cap) in practice. Thus, the minimization of the maximum settlement and differential settlement for a GRPS embankment can be achieved using the typical pile spacing mentioned above. Additionally, variations in pile length are also a major concern when designing a GRPS embankment. As discussed previously, the embankment failure in the engineering case was mainly caused by insufficient pile length, instead of by the spacing and location of the rigid piles. Therefore, this study primarily focused on the effect of the pile length on the stability of the GRPS embankment.

To evaluate the influence of varying pile lengths (L) on the maximum lateral movement of the floating pile (at an embankment height of 6.0 m), ten values of L were examined: 15, 15.5, 16, 16.5, 17, 17.5, 18, 18.5, 19, 19.5 m, as depicted in Fig. 14a. Note that the pile length L in the figure was normalized concerning the thickness of soft soil layer h_0. As anticipated, the lateral movement of the floating pile apparently decreased as the pile length increased. Specifically, for the floating pile with a L/h_0 of 0.8, the
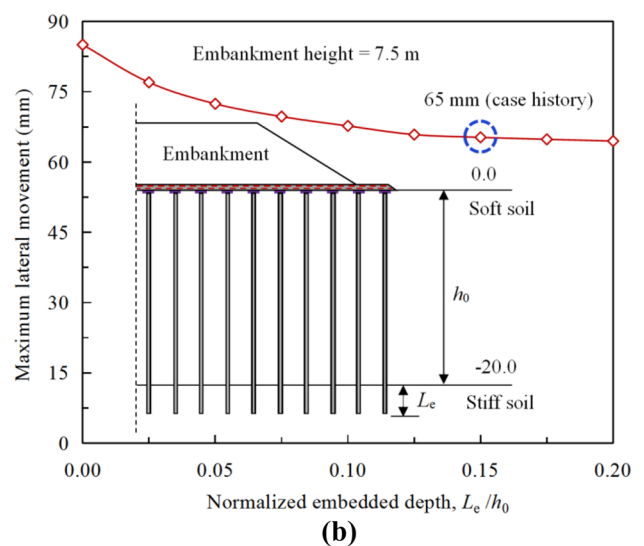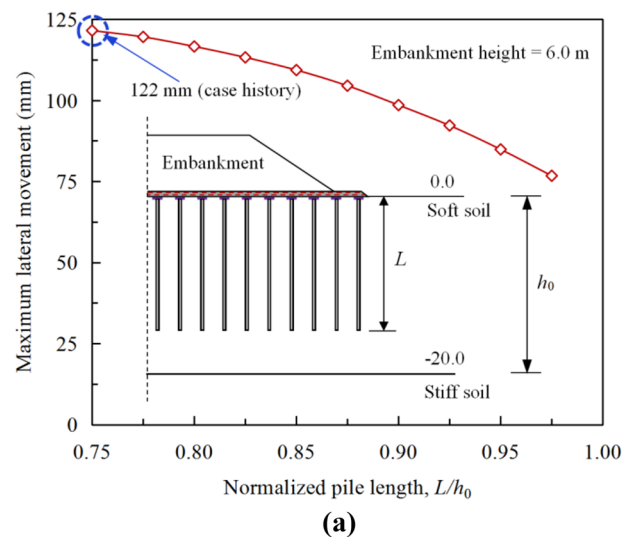

(a)

(b)

Fig. 14 Effect of pile length on the maximum lateral movement of the **a** floating and **b** end-bearing piles

maximum lateral movement was found to be 117 mm, which was approximately 1.5 times greater than the maximum lateral movement observed in the case of the floating pile with a L/h_0 of 0.975. This result can be ascribed to the fact that an increase in the length of the floating pile contributes to an obvious elevation in the bearing resistance of pile. As expected, a higher pile-bearing resistance can noticeably increase the load transferred from the soft soils to the floating pile and thus significantly reduce the lateral soil pressure acting on the passive pile, which induces smaller pile deflection. Moreover, as the strength of soft soils increases with depth, the slight embedment effect of the longer floating pile contributes to a reduction in the lateral movement. Consequently, it can be concluded that increasing the length of the floating pile will significantly change the lateral behavior of the pile and may be regarded

as an effective method in improving GRPS embankment stability. Therefore, when using floating piles in a GRPS embankment system, careful consideration should be given to pile length to ensure embankment stability.

To further study the effect of embedded length of the end-bearing pile (L_e) at an embankment height of 7.5 m, various L_e of the pile were considered. The embedded depths considered were 0–4.0 m, corresponding to pile lengths of 20–24 m, respectively. It is worth mentioning that for the end-bearing piles, an embedded depth of 0 m denotes that the tips of the piles were located slightly above the stiff soil layer. The maximum lateral movement of the end-bearing pile is plotted against the normalized embedded depth L_e/h_0 in Fig. 14b. As L_e/h_0 increased, the lateral movement of piles slightly reduced. This reduction was only somewhat significant as L_e/h_0 varied from 0 to 0.15. However, the rate of reduction was approximately constant when L_e/h_0 exceeded 0.15. This may imply that once the embedded pile length exceeds a particular threshold, additional increases in pile length may no longer be effective in the reduction of the lateral movement because of the already sufficient embedment of the end-bearing pile in the stiff soil layer. The results also demonstrate that the embedded length of the end-bearing pile plays a relatively less vital role in the lateral movement of piles compared with the length of the floating piles. As a result, it is unnecessary to ensure a large embedded length in the stiff soil layer when adopting end-bearing piles in a GRPS embankment system.

Like other foundation systems, rigid pile foundations are limited in supporting a certain height of the geosynthetic-reinforced embankment. According to Huang and Han [38], the critical height corresponds to a sudden nonlinear increase in the maximum settlement and lateral displacement versus the embankment height plot. The computed critical height of embankment versus the normalized pile length L/h_0 is illustrated in Fig. 15, which shows that a longer pile length yielded a higher critical height. When L/h_0 varied from 0.75 to 1.15, the critical height increased from 6.2 to 11.8 m. This effect is mainly attributed to the fact that a longer pile length leads to a smaller lateral movement on the piles. Consequently, the rigid piles can support more embankment loads as the pile length increases. In other words, the stability of the GRPS embankment may be markedly enhanced by increasing the pile length, especially in the case of a geosynthetic-reinforced embankment supported on floating piles. From Fig. 15, it is observed that when the normalized pile length was over 1.15 (i.e., the normalized embedded length of pile was 0.15), the critical height stabilized with negligible variation. This also suggests that the overall safety factor of the GRPS embankment will gradually approach a constant with the increasing embedded length of the end-bearing pile.
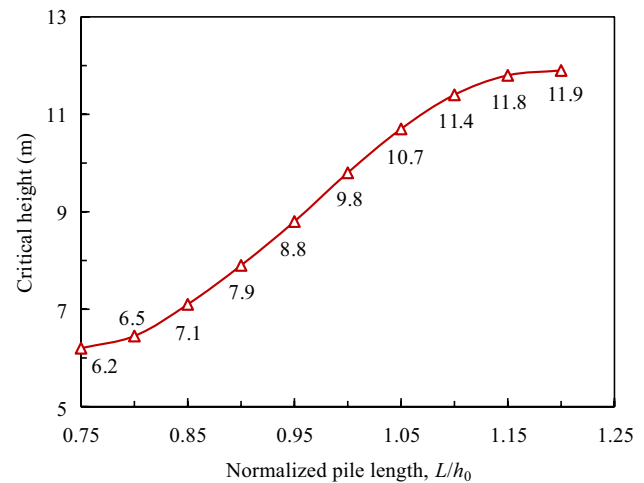

Fig. 15 Critical height of embankment versus normalized pile length response

In summary, the premature failure of the GRPS embankment over soft soils may always be induced by inclination or bending failure of rigid piles instead of shear failure. However, at present, it is still quite commonplace to use limit equilibrium approaches that neglect to consider these lateral failure modes of rigid piles to evaluate the overall stability of GRPS embankments, as suggested by the relevant design specifications [27, 28]. In other words, current design procedures regarding the stability analysis of GRPS embankments do not incorporate the effects of the inclination or bending failure mode, but only consider the shear failure mode, which may greatly overestimate the stability of the GRPS embankments. Moreover, the lateral behavior and failure modes of rigid piles under geosynthetic-reinforced embankment were revealed to exhibit significant dependence on pile length. It is imperative for this aspect to be carefully considered in the current design practice. Therefore, to accurately evaluate the GRPS embankment stability, current design practice should be improved to include the effect of the length of rigid piles. Additionally, due to the complexity of the problem itself, it is recommended the 3D numerical modeling be incorporated into the stability design of GRPS embankments to achieve reliable designs.

6 Summary and Conclusions

This paper described a case history of a GRPS highway embankment project that failed to be constructed over soft clay. Based on this engineering case, 3D FE analyses involving the pile–soil and geosynthetic-gravel interactions were conducted to investigate the lateral responses and failure modes of floating and end-bearing piles in soft soils under geosynthetic-reinforced embankments. This paper also

examined the influences of geosynthetic reinforcement and pile length on the stability of the embankment. The main conclusions derived from this study are as follows:

1. Under identical embankment loading, the induced lateral responses in the floating and end-bearing piles are significantly different. Specifically, the lateral movement of the floating pile is markedly larger than that of the end-bearing pile, while the maximum moment of the floating pile is evidently smaller than that of the end-bearing pile.

2. Under embankment loading, inclination failure occurs in the floating pile instead of shear and bending failure. However, in the case of the end-bearing pile, bending failure is the main mode of failure, which is more likely to occur at or near the interface between the alternating soft and stiff soil layers.

3. The inclusion of geosynthetic reinforcement can enhance the stability of piled embankments to some extent. However, an increase in the length of the floating pile contributes significantly toward improving the stability against inclination failure of the pile. According to the numerical results, with an increase in normalized pile length from 0.8 to 0.975, the reduction of the maximum lateral movement of the floating pile is estimated to be 33% at an embankment height of 6.0 m. Furthermore, when the normalized pile length varies from 0.75 to 1.15, the critical height of embankment increases from 6.2 to 11.8 m. Nevertheless, the influence of pile length becomes less important once the normalized pile length exceeds 1.15.

4. The lateral response and failure modes of the rigid piles in GRPS embankment systems are extraordinarily dependent on pile length. Therefore, it is vital to include the effect of the pile length when calculating the GRPS embankment stability.

References

1. Han J, Gabr MA (2002) Numerical analysis of geosynthetic-reinforced and pile-supported earth platforms over soft soil. J Geotech Geoenviron Eng ASCE 128(1):44–53

2. Borges JL, Marques DO (2011) Geosynthetic-reinforced and jet grout column-supported embankments on soft soils: numerical analysis and parametric study. Comput Geotech 38(7):883–896

3. Jamsawang P, Yoobanpot N, Thanasisathit N, Voottipruex P, Jongpradist P (2016) Three-dimensional numerical analysis of a DCM column-supported highway embankment. Comput Geotech 72:42–56

4. Chen YM, Cao WP, Chen RP (2008) An experimental investigation of soil arching within basal reinforced and unreinforced piled embankments. Geotext Geomembr 26(2):164–174

5. Liu HL, Ng CWW, Fei K (2007) Performance of a geogrid-reinforced and pile-supported highway embankment over soft clay: case study. J Geotech Geoenviron Eng ASCE 133(12):1483–1493

6. Oh YI, Shin EC (2007) Reinforcement and arching effect of geogrid-reinforced and pile-supported embankment on marine soft ground. Mar Georesour Geotechnol 25(2):97–118

7. Zhang CL, Jiang GL, Liu XF, Buzzi O (2016) Arching in geogrid-reinforced pile-supported embankments over silty clay of medium compressibility: field data and analytical solution. Comput Geotech 77:11–25

8. Fagundes DF, Almeida MSS, Thorel L, Blanc M (2017) Load transfer mechanism and deformation of reinforced piled embankments. Geotext Geomembr 45(2):1–10

9. Zheng G, Jiang Y, Han J, Liu YF (2011) Performance of cement-fly ash-gravel pile-supported high-speed railway embankments over soft marine clay. Mar Georesour Geotechnol 29(2):145–161

10. Briançon L, Simon B (2011) Performance of pile-supported embankment over soft soil: full-scale experiment. J Geotech Geoenviron Eng ASCE 138(4):551–561

11. Cao WZ, Zheng JJ, Zhang J, Zhang RJ (2016) Field test of a geogrid-reinforced and floating pile-supported embankment. Geosynth Int 23(5):348–361

12. Huang J, Han J, Oztoprak S (2009) Coupled mechanical and hydraulic modeling of geosynthetic-reinforced column-supported embankments. J Geotech Geoenviron Eng ASCE 135(8):1011–1021

13. Jones BM, Plaut RH, Filz GM (2010) Analysis of geosynthetic reinforcement in pile-supported embankments. Part I: 3D plate model. Geosynth Int 17(2):59–67

14. Han J, Bhandari A, Wang F (2012) DEM analysis of stresses and deformations of geogrid-reinforced embankments over piles. Int J Geomech 12(4):340–350

15. Zhuang Y, Ellis E (2014) Finite-element analysis of a piled embankment with reinforcement compared with BS 8006 predictions. Geotechnique 64(11):910–917

16. Abusharar SW, Zheng JJ, Chen BG, Yin JH (2009) A simplified method for analysis of a piled embankment reinforced with geosynthetics. Geotext Geomembr 27(1):39–52

17. Zhou WH, Chen RP, Zhao LS, Xu ZZ, Chen YM (2012) A semi-analytical method for the analysis of pile-supported embankments. J Zhejiang Univ Sci A 13(11):888–894

18. Ariyarathne P, Liyanapathirana DS (2015) Review of existing design methods for geosynthetic-reinforced pile-supported embankments. Soils Found 55(1):17–34

19. Fonseca ECA, Palmeira EM (2018) An evaluation of the accuracy of design methods for geosynthetic reinforced piled embankments. Can Geotech J. https://doi.org/10.1139/cgj-2018-0071

20. Ardalan H, Eslami A, Nariman-Zadeh N (2009) Piles shaft capacity from CPT and CPTu data by polynomial neural networks and genetic algorithms. Comput Geotech 36(4):616–625

21. Baziar MH, Kashkooli A, Azizkandi AS (2012) Prediction of pile shaft resistance using cone penetration tests (CPTs). Comput Geotech 45:74–82

22. Kordjazi A, Nejad FP, Jaksa MB (2014) Prediction of ultimate axial load-carrying capacity of piles using a support vector machine based on CPT data. Comput Geotech 55:91–102

23. Li HJ, Liu SY, Tong LY (2019) Evaluation of lateral response of single piles to adjacent excavation using data from cone penetration tests. Can Geotech J 56(2):236–248

24. Su Q, Huang JJ (2013) Deformation and failure modes of composite foundation with sub-embankment plain concrete piles. Sci Cold Arid Regions 5(5):614–625

25. Yu JL, Zhong JN, Li JY, Xu RQ, Gong XN (2018) Centrifugal model tests on working behavior of composite foundation reinforced by rigid piles with caps under embankment. In: Proceedings of China–Europe conference on geotechnical engineering, Vienna, pp 1077–1080

26. Zheng G, Yang XY, Zhou HZ, Chai JC (2018) Numerical modeling of progressive failure of rigid piles under an embankment load. Can Geotech J. https://doi.org/10.1139/cgj-2017-0613

27. British standard (BS) 8006-1 (2010) Code of practice for strengthened/reinforced soils and other fills. British Standards Institution (BSI), London

28. JTG D30–2015 (2015) Specification for design of highway subgrades. China Communications Press, Beijing

29. Oliveira PJV, Pinheiro JL, Correia AA (2011) Numerical analysis of an embankment built on soft soil reinforced with deep mixing columns: parametric study. Comput Geotech 38(4):566–576

30. Chai JC, Shrestha S, Hino T, Ding WQ, Kamo Y, Carter J (2015) 2D and 3D analyses of an embankment on clay improved by soil-cement columns. Comput Geotech 68:28–37

31. Wu JT, Ye X, Li J, Li JW (2019) Field and numerical studies on the performance of high embankment built on soft soil reinforced with PHC piles. Comput Geotech 107:1–13

32. Zhang J, Zheng JJ, Chen BG, Yin JH (2013) Coupled mechanical and hydraulic modeling of a geosynthetic-reinforced and pile-supported embankment. Comput Geotech 52(1):28–37

33. Rowe RK, Liu KW (2015) Three-dimensional finite element modelling of a full-scale geosynthetic-reinforced, pile-supported embankment. Can Geotech J 52(12):2041–2054

34. Bhasi A, Rajagopal K (2015) Numerical study of basal reinforced embankments supported on floating/end bearing piles considering pile-soil interaction. Geotext Geomembr 43(6):524–536

35. Kitazume M, Maruyama K (2007) External stability of group column type deep mixing improved ground under embankment loading. Soils Found 47(3):437–455

36. Shrestha S, Chai JC, Bergado DT, Hino T, Kamo Y (2016) 3D FEM investigation on bending failure mechanism of column inclusion under embankment Load. Lowland Technol Int 17(3):157–166

37. Lai HJ, Zheng JJ, Zhang J, Zhang RJ, Cui L (2014) DEM analysis of "soil"-arching within geogrid-reinforced and unreinforced pile-supported embankments. Comput Geotech 61:13–23

38. Huang J, Han J (2008) Critical height of deep mixed column-supported embankment under an undrained condition. In: Proceedings of geocongress 2008: geosustainability and geohazard mitigation, New Orleans, pp 638–645